This article has been accepted for publication in a future issue of this journal, but has not been fully edited. Content may change prior to final publication. Citation information: DOI 10.1109/JPHOT.2021.3123168, IEEE Photonics Journal

Photonic Techniques for Generating a Single RF Sideband With No Second Order Sidebands

Chongjia Huang and Erwin H. W. Chan, *Senior Member, IEEE*

***Abstract*—Two structures that can realise optical single sideband modulation without generating both second order upper and lower sidebands are presented. They are based on a dual-parallel Mach Zehnder modulator (DP-MZM) with an optical filter and a dual-polarisation dual-parallel Mach Zehnder modulator (DPol-DPMZM) with a 90° hybrid coupler. The former is an all-optical structure and hence it has a very wide bandwidth. The latter uses one DP-MZM to realise single sideband suppressed carrier modulation while the other DP-MZM simply passes the optical carrier. It also suppresses the third order sideband on the same side as the wanted fundamental RF modulation sideband. Hence, in an ideal situation, there is no second order harmonic component generated after photodetection. Experimental results are presented for the novel structures, which demonstrate the realisation of optical single sideband modulation without second order sidebands. The results also show large fundamental to second order harmonic power ratio over a wide input RF signal frequency range even after inserting a long single mode fibre into the system for signal transmission. The new optical single sideband modulators find applications in improving the multioctave spurious free dynamic range in a long-haul fibre optic link and reducing measurement errors in an optical vector analyser.**

***Index Terms*—Optical single-sideband modulation, electro-optic modulators, radio over fibre (RoF), optical vector network analyser.**

I. Introduction

Many applications require a system that generates an optical carrier and a single RF modulation sideband. A classic example is to avoid the chromatic dispersion problem and to improve the spectrum efficiency in optical communication [1]. Another example is to implement an optical vector analyser to determine the magnitude and phase response of an optical component [2]. Optical single sideband (OSSB) modulation is also used in sensing, wavelength conversion and signal processing.

There are two conventional approaches for realising OSSB modulation. They are based on using an optical filter to remove either the upper or lower sidebands generated by a Mach Zehnder modulator (MZM) or a phase modulator [3], and connecting a 90° hybrid coupler to the input RF ports of a quadrature-biased dual-drive MZM (DDMZM) [1]. Since an optical modulator is a nonlinear device, the second and higher order sidebands are also generated. In the case of optical communication, chromatic dispersion in fibre introduces phase shifts to the sidebands. The phase shifts in the second order sidebands caused by chromatic dispersion results in the second order harmonic component appears at the output of a fibre optic link implemented by a conventional DDMZM based OSSB modulator. The amplitude of this second order harmonic component is dependent on the input RF signal frequency. This problem remains in the conventional optical filter based OSSB modulator. This is because, when using an optical filter to remove the lower sidebands for example, the second order harmonic component can still be generated by the optical carrier beats with the second order upper sideband at the photodetector, as well as the beating of the first and third order upper sidebands. Suppressing the second order harmonic is needed in multioctave bandwidth fibre optic links [4], which has applications including antenna remoting, ultra-wideband analog communications and RF distribution systems for defence platforms [5]. In an optical vector analyser, the second and higher order sidebands cause measurement errors [6].

The above examples show the need of suppressing the unwanted sidebands in an OSSB modulator. Several approaches have been proposed [7]-[10] to suppress the second order sidebands but only two of them provide experimental verification. One approach is to apply two 120° phase difference RF signals into the two RF ports of a DDMZM [7]. It has the drawback of a 120° coupler is not a standard electrical component. A wideband 120° coupler is not commercially available. Furthermore, it only suppresses one second order sideband. A second order harmonic component is generated when the carrier beats with the remaining second order sideband at the photodetector. Another approach is based on a dual-parallel MZM (DP-MZM) [8]. It has the drawback of requiring a power splitter and two electrical couplers. Although these are standard electrical components and broadband power splitters and couplers are commercially available, it is difficult to maintain large unwanted sideband suppression over a wide frequency range due to the amplitude and phase imbalance in the couplers.

Two structures for OSSB modulation without generating second order sidebands are presented. The first structure is based on a DP-MZM with no electrical components. Therefore it can operate over a wide frequency range where the upper operating frequency is only limited by the optical modulator bandwidth. The second structure is based on operating a DP-MZM inside a dual-polarisation dual-parallel MZM (DPol-DPMZM) as a single-sideband suppressed-carrier

Manuscript received August 24, 2021. *(Corresponding author: Erwin H. W. Chan)*

Chongjia Huang and Erwin H. W. Chan are with College of Engineering, IT and Environment, Charles Darwin University, Darwin NT 0909, Australia. (e-mail: erwin.chan@cdu.edu.au).

This article has been accepted for publication in a future issue of this journal, but has not been fully edited. Content may change prior to final publication. Citation information: DOI 10.1109/JPHOT.2021.3123168, IEEE Photonics Journal

modulator. It not only has the advantage of no second order sidebands, but under an ideal situation, no second order harmonic component is generated after photodetection. Experimental results demonstrate the realisation of OSSB modulation with the second order sidebands of more than 38 dB below the fundamental RF modulation sideband for 0.5 modulation index. This is an over 21 dB improvement compared to the conventional OSSB modulator based on a DDMZM with a 90° hybrid coupler operating under the same condition. Large fundamental to second order harmonic power ratio of around 40 dB over an input RF signal frequency range of 3 to 13 GHz is also demonstrated using the two new OSSB modulation structures with a 20.3 km standard single mode fibre for signal transmission.

II. Topologies and Operation Principle

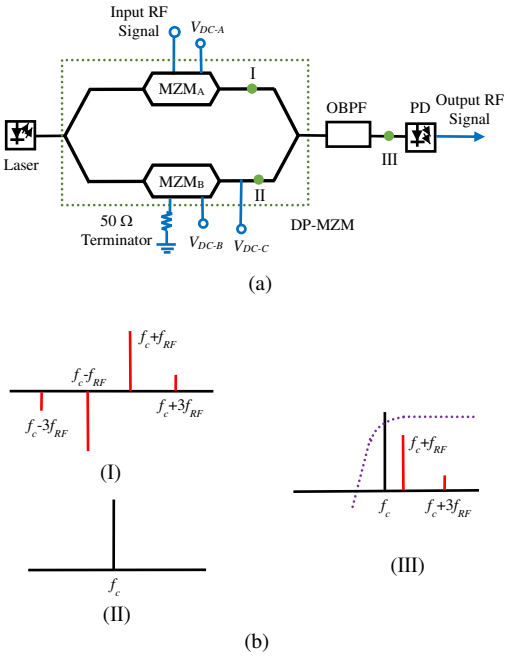

Fig. 1. (a) Structure of the DP-MZM based optical single sideband modulator. (b) Optical spectrums at different locations of the modulator. The dotted line is the optical bandpass filter magnitude response. f_c and f_{RF} are the frequency of the optical carrier and the input RF signal respectively.

The topology of the new OSSB modulator without second order sidebands is depicted in Fig. 1(a). It is based on a DP-MZM, which comprises two single-drive MZMs (MZM$_A$ and MZM$_B$) connected in parallel inside a main MZM, followed by an optical bandpass filter (OBPF). Each sub-MZM in the DP-MZM has an RF port for RF signal modulation and a DC port for setting the modulator operating point. Continuous wave light from a laser source is launched into the DP-MZM. MZM$_A$ in the DP-MZM is driven by an RF signal and is biased at the null point for double-sideband suppressed-carrier modulation. As shown in Fig. 1(bI), the optical spectrum at MZM$_A$ output contains two first order RF modulation sidebands at $f_c \pm f_{RF}$ and two third order RF modulation sidebands at $f_c \pm 3f_{RF}$. The optical carrier and the even order sidebands are eliminated under an ideal situation. MZM$_B$ is biased at the peak point and its RF port is terminated by a 50 Ω terminator. Only an optical carrier at f_c is present at the output of MZM$_B$ as shown in Fig. 1(bII). Note that MZM$_B$ can be eliminated as it simply lets the continuous wave light to pass through the bottom arm of the main MZM in the DP-MZM. This simplifies the structure and reduces the number of DC bias voltage. However, an optical modulator formed by an MZM in only one arm of a main MZM is not commercially available. Hence, MZM$_B$ was included in the structure even though it does not provide any function to the DP-MZM based OSSB modulator. The main MZM in the DP-MZM is biased at the peak point. An OBPF is connected to the DP-MZM output to filter out the lower RF modulation sidebands. Fig. 1(bIII) shows the optical spectrum after the OBPF, which contains the optical carrier, and the first and third order upper RF modulation sidebands. The structure shown in Fig. 1(a) does not generate both second order upper and lower sidebands and does not require any electrical component, which is clearly an advantage compared to the structures presented in [7] that uses a 120° coupler to split an RF signal and in [8] that involves a 90° hybrid coupler and a 180° hybrid coupler.

The electric field of the optical signal at the OBPF output can be expressed as

$$E_{DPMZM,out}(t) = \frac{1}{2} E_{in} \sqrt{t_{ff}} e^{j\omega_c t} \left(1 + J_1(m_{RF}) e^{j\omega_{RF} t} + J_3(m_{RF}) e^{j3\omega_{RF} t}\right) \quad (1)$$

where E_{in} is the electric field amplitude of the continuous wave light into the DP-MZM, t_{ff} is the insertion loss of the DP-MZM, $\omega_c = 2\pi f_c$ and $\omega_{RF} = 2\pi f_{RF}$ are the angular frequency of the optical carrier and the input RF signal respectively, $J_n(x)$ is the Bessel function of nth order of the first kind, $m_{RF} = \pi V_{RF} / V_{\pi,DPMZM}$ is the RF modulation index, V_{RF} is the input RF signal voltage and $V_{\pi,DPMZM}$ is the DP-MZM RF port switching voltage. The optical carrier and the first and third order upper sidebands at the OBPF output are detected by a photodetector (PD). The PD generates a photocurrent at the RF signal frequency, which can be obtained from (1), and is given by

$$I_{DPMZM,RF}(t) = \frac{1}{2} P_{in} t_{ff} \Re J_1(m_{RF}) \cos(\omega_{RF} t) \quad (2)$$

where $\Re$ is the PD responsivity and P_{in} is the continuous wave light power into the DP-MZM. Note that a second order harmonic component is also generated. This is due to the first order sideband beats with the third order sideband at the PD. The photocurrent at the second order harmonic frequency is given by

$$I_{DPMZM,2RF}(t) = \frac{1}{2} t_{ff} P_{in} \Re J_1(m_{RF}) J_3(m_{RF}) \cos(2\omega_{RF} t) \quad (3)$$

In long-haul fibre optic links or antenna remoting applications, the transmission distance can be in the order of 20 km [11], [12]. A single mode fibre (SMF) is inserted after the OBPF in the OSSB modulator structure shown in Fig. 1(a) to investigate the chromatic dispersion effect on the output RF signal and the second order harmonic component. The phase shift introduced by the chromatic dispersion to the nth order sideband is given by [1]

$$\varphi_n = \frac{\pi LD}{c}\lambda_c^{\,2}\left(nf_{RF}\right)^2 \tag{4}$$

where L is the fibre length, λ_c is the optical carrier wavelength, c is the speed of light in vacuum and D is the fibre dispersion parameter. With the inclusion of the phase shift φ_n to the sidebands, the photocurrents at the fundamental RF signal frequency and the second order harmonic frequency become

$$I'_{DPMZM,RF}(t) = \frac{1}{2}t_{ff}P_{in}\Re J_1(m_{RF})\cos(\omega_{RF}t+\varphi_1) \tag{5}$$

$$I'_{DPMZM,2RF}(t) = \frac{1}{2}t_{ff}P_{in}\Re J_1(m_{RF})J_3(m_{RF})\cos(2\omega_{RF}t+\varphi_3-\varphi_1) \tag{6}$$

It can be seen from (5) and (6) that chromatic dispersion has no effect on the two photocurrent amplitudes.

As a comparison, the conventional OSSB modulator based on a 90° hybrid coupler at the inputs of a DDMZM was analysed up to and including the third order sidebands. A phase shift introduced by chromatic dispersion to each sideband was included in the analysis. The photocurrents at the fundamental RF signal frequency and the second order harmonic frequency are given by

$$I'_{DDMZM,RF}(t) = \sqrt{2}t_{ff}P_{in}\Re\begin{bmatrix} -J_0(m_{RF})J_1(m_{RF})\cos\left(\omega_{RF}t-\varphi_1+\frac{\pi}{4}\right) \\ -J_2(m_{RF})J_1(m_{RF})\cos\left(\omega_{RF}t+\varphi_1-\varphi_2+\frac{\pi}{4}\right) \\ +J_2(m_{RF})J_3(m_{RF})\cos\left(\omega_{RF}t-\varphi_2+\varphi_3+\frac{\pi}{4}\right) \end{bmatrix} \tag{7}$$

$$I'_{DDMZM,2RF}(t) = 2t_{ff}P_{in}\Re J_0(m_{RF})J_2(m_{RF})\sin(\varphi_2)\cos(2\omega_{RF}t) \tag{8}$$

(7) show beating of the second order sideband with the first and third order sidebands also generate a frequency component at the RF signal frequency. These frequency components affect the output RF signal produced by the beating of the carrier and the first order sideband. Since φ_n is dependent on the input RF signal frequency, the conventional OSSB modulator has a frequency-dependent output RF signal amplitude. Note that the two second order sidebands generated by the conventional OSSB modulator are out of phase. Hence, without the effect of chromatic dispersion, no second order harmonic component is present at the link output. However, chromatic dispersion in a long-haul fibre optic link alters the sideband phases, which causes the presence of the second order harmonic with a frequency-dependent amplitude as shown in (8).

In the second OSSB modulator topology [Fig. 2(a)], the RF signal is applied to a DPol-DPMZM. The DPol-DPMZM comprises a 3-dB optical coupler, two DP-MZMs (DP-MZM$_X$ and DP-MZM$_Y$), a 90° polarisation rotator (PR) and a polarisation beam combiner (PBC). Each DP-MZM has two RF ports and three DC ports. DP-MZM$_X$ is driven by two 90° phase difference RF signals and is biased to obtain single-sideband suppressed-carrier (SSB-SC) modulation [13]. As shown in Fig. 2(bI), the output of an SSB-SC modulator consists of the third order lower RF modulation sideband at f_c-3f_{RF} and the first order upper RF modulation sideband at f_c+f_{RF} under an ideal situation. The RF ports of DP-MZM$_Y$ are terminated by 50 Ω terminators. The three bias points of DP-MZM$_Y$ are set at the peak point to enable the optical carrier to pass through the modulator with minimal loss. The polarisation state of the optical carrier at the output of DP-MZM$_Y$ is rotated by 90° via a PR. The two orthogonally polarised optical signals are combined by a PBC. The output of the DPol-DPMZM is connected to an in-line polariser with a 45° angle to the slow axis. This ensures the two orthogonally polarised optical signals have the same polarisation state before detected by a PD. Fig. 2(bIII) shows the DPol-DPMZM output optical spectrum consists of an optical carrier, the first order upper RF modulation sideband and the third order lower RF modulation sideband. Both the upper and lower second order sidebands are eliminated. Compared to the structures presented in [7] and [8], the DPol-DPMZM based OSSB modulator has the advantage of only a single standard electrical coupler is needed. Since the third order sideband on the same side as the wanted first order sideband is eliminated, there is no second order harmonic component generated after photodetection. On the other hand, the output of the OSSB modulators in [7] and Fig. 1(a) contains the second order harmonic component.

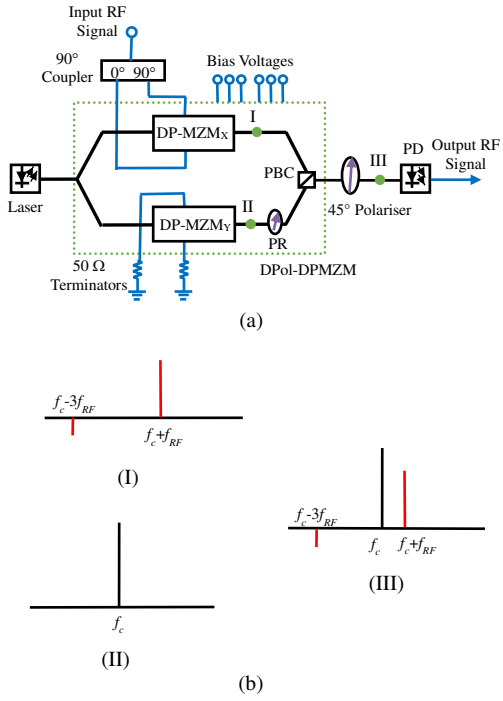

Fig. 2. (a) Structure of the DPol-DPMZM based optical single sideband modulator. (b) Optical spectrums at different locations of the modulator.

In practice, a 90° hybrid coupler, which is used to split an RF signal into two with a 90° phase difference, has phase imbalance. We include a 90° hybrid coupler phase imbalance θ in the analysis. The DPol-DPMZM based OSSB modulator output electric field can be expressed as

This article has been accepted for publication in a future issue of this journal, but has not been fully edited. Content may change prior to final publication. Citation information: DOI 10.1109/JPHOT.2021.3123168, IEEE Photonics Journal

$$E_{DPol-DPMZM_{out}}(t)=\frac{1}{4}E_{in}\sqrt{t_{ff}}e^{j\omega_c t}\cdot\begin{bmatrix}2+(j+je^{j\theta})J_1(m_{RF})e^{j\omega_{RF}t}+(-j+je^{-j\theta})J_1(m_{RF})e^{-j\omega_{RF}t}\\+(j-je^{j3\theta})J_3(m_{RF})e^{j3\omega_{RF}t}+(-j-je^{-j3\theta})J_3(m_{RF})e^{-j3\omega_{RF}t}\end{bmatrix} \tag{9}$$

The additional sidebands at f_c-f_{RF} and f_c+3f_{RF} with electric field amplitudes given by the third and fourth terms inside the square brackets in (9) are due to the 90° hybrid coupler phase imbalance. The second order sidebands remain cancelled even the 90° hybrid coupler has a phase imbalance. The output optical signal is detected by a PD. Beating of the optical carrier and the RF modulation sidebands at the PD generate an output RF signal and the second order harmonic component. Their photocurrents are given by

$$I_{DPol-DPMZM,RF}(t)=-\frac{1}{2}t_{ff}P_{in}\Re J_1(m_{RF})\sin(\omega_{RF}t) \tag{10}$$

$$I_{DPol-DPMZM,2RF}(t)=\begin{bmatrix}\frac{1}{4}t_{ff}P_{in}\Re\sin(\theta)\left(2J_1(m_{RF})J_3(m_{RF})-J_1^{\,2}(m_{RF})\right)\\\cdot\cos(2\omega_{RF}t+\phi)\end{bmatrix} \tag{11}$$

where

$$\phi=\tan^{-1}\left(\frac{1-\cos(2\theta)}{\sin(2\theta)}\right) \tag{12}$$

(11) shows the DPol-DPMZM based OSSB modulator generates the second order harmonic component when the 90° hybrid coupler has phase imbalance. As in the DP-MZM based OSSB modulator, we include a phase shift φ_n due to chromatic dispersion to the nth order sidebands of the DPol-DPMZM based OSSB modulator. The photocurrents at the fundamental RF signal frequency and the second order harmonic frequency become

$$I'_{DPol-DPMZM,RF}(t)=\begin{bmatrix}-\frac{1}{2}t_{ff}P_{in}\Re J_1(m_{RF})\sqrt{1-\sin(\theta)\sin(2\varphi_1)}\\\cdot\sin\left(\omega_{RF}t+\tan^{-1}\left(\frac{\tan(\varphi_1)\cos(\theta)}{1-\tan(\varphi_1)\sin(\theta)}\right)\right)\end{bmatrix} \tag{13}$$

$$I'_{DPol-DPMZM,2RF}(t)=\frac{1}{4}t_{ff}P_{in}\Re\cdot\begin{bmatrix}\begin{bmatrix}\frac{1}{2}J_1^{\,2}(m_{RF})\left(\cos(2\theta)-1\right)+J_1(m_{RF})J_3(m_{RF})\\\cdot\begin{bmatrix}\cos(\varphi_3-\varphi_1)\left(1-\cos(2\theta)\right)+\\\sin(\varphi_3-\varphi_1)\left(\sin(3\theta)+\sin(\theta)\right)\end{bmatrix}\end{bmatrix}\cos(2\omega_{RF}t)\\+\begin{bmatrix}-\frac{1}{2}J_1^{\,2}(m_{RF})\sin(2\theta)+J_1(m_{RF})J_3(m_{RF})\\\cdot\begin{bmatrix}\sin(\varphi_3-\varphi_1)\left(\cos(3\theta)-\cos(\theta)\right)\\+\cos(\varphi_3-\varphi_1)\sin(2\theta)\end{bmatrix}\end{bmatrix}\sin(2\omega_{RF}t)\end{bmatrix} \tag{14}$$

(13) shows, when the 90° hybrid coupler has phase imbalance, i.e. $\theta\neq0°$, chromatic dispersion affects the DPol-DPMZM based OSSB modulator output RF signal amplitude. However, the effect is small for few-degree 90° hybrid coupler phase imbalance.

III. Simulation Results and Discussion

The ratio of the output RF signal power to the second order harmonic power of the DP-MZM based OSSB modulator can be obtained from (5) and (6). It was plotted versus the modulation index and is depicted by a solid line in Fig. 3(a). The output RF signal to the second order harmonic power ratio of the conventional DDMZM based OSSB modulator, which can be obtained from (7) and (8), is also depicted by a dashed line in the figure for comparison. It was plotted under the worst-case scenario where the second order harmonic component, caused by the chromatic dispersion effect, has a maximal amplitude. The figure shows, for a modulation index of less than 0.8, the DP-MZM based OSSB modulator has an over 40 dB fundamental to second order harmonic power ratio, which results in over 29 dB power ratio improvement compared to the conventional DDMZM based OSSB modulator.

In practice, there are loss imbalance and modulation efficiency imbalance in the two arms of an MZM [14]. We included these two imbalances in the DP-MZM based OSSB modulator analysis. The photocurrents at the fundamental RF signal frequency and the second order harmonic frequency in (5) and (6) become

$$\begin{aligned}I''_{DPMZM,RF}(t)=\frac{1}{8}t_{ff}P_{in}\Re\Big\{&\left[\left(1+\gamma\right)+\gamma J_0(m_{RF1})-J_0(m_{RF2})\right]\\&\times\left[\gamma J_1(m_{RF1})+J_1(m_{RF2})\right]\cos(\omega_{RF}t+\varphi_1)\\&+\left[\gamma J_2(m_{RF1})-J_2(m_{RF2})\right]\\&\times\left[\gamma J_3(m_{RF1})+J_3(m_{RF2})\right]\cos(\omega_{RF}t+\varphi_2-\varphi_3)\Big\}\end{aligned} \tag{15}$$

$$\begin{aligned}I''_{DPMZM,2RF}(t)=\frac{1}{8}t_{ff}P_{in}\Re\Big\{&\left[\left(1+\gamma\right)+\gamma J_0(m_{RF1})-J_0(m_{RF2})\right]\\&\times\left[\gamma J_2(m_{RF1})-J_2(m_{RF2})\right]\cos(2\omega_{RF}t+\varphi_2)\\&+\left[\gamma J_1(m_{RF1})+J_1(m_{RF2})\right]\\&\times\left[\gamma J_3(m_{RF1})+J_3(m_{RF2})\right]\cos(2\omega_{RF}t-\varphi_1+\varphi_3)\Big\}\end{aligned} \tag{16}$$

where m_{RF1} and m_{RF2} are the RF modulation index in arm 1 and arm 2 of MZM_A,

$$\gamma=\frac{\varepsilon^{1/2}-1}{\varepsilon^{1/2}+1} \tag{17}$$

and ε is the modulator extinction ratio. Using the auxiliary angle method to rearrange (15) and (16) shows that chromatic dispersion in a SMF affects the amplitude of the DP-MZM based OSSB modulator output RF signal and second order harmonic component. Simulation was conducted using (15)-(17) with typical x cut MZM parameters of ε=30 dB and α=0.05 where α is the chirp parameter representing the amount of modulation efficiency imbalance that causes different RF modulation indexes (m_{RF1}, m_{RF2}) in the two arms of MZM_A. The result shows the DP-MZM based OSSB modulator fundamental to second order harmonic power ratio is in the range of 39.8 dB and 44.9 dB for an input RF signal frequency of below 20 GHz and an RF modulation index of 0.5. The DP-MZM based OSSB modulator fundamental to second order harmonic power ratio as a function of the RF modulation index

This article has been accepted for publication in a future issue of this journal, but has not been fully edited. Content may change prior to final publication. Citation information: DOI 10.1109/JPHOT.2021.3123168, IEEE Photonics Journal

is shown by a dash-dotted line in Fig. 3(a). It was plotted under the worst-case scenario that results in the smallest power ratio after including the loss and modulation efficiency imbalances (ε=30 dB and α=0.05) in the simulation. The result shows over 22.5 dB power ratio improvement compared to the conventional DDMZM based OSSB modulator can still be obtained in practice when the modulation index is less than 0.8.

Fig. 3(b) depicts the ratio of the output RF signal power to the second order harmonic power of the DPol-DPMZM based OSSB modulator as a function of the modulation index, when the 90° hybrid coupler has a ±0.5°, ±1°, ±2°, ±3° and ±4° phase imbalance. It can be seen from the figure that more than 40 dB fundamental to second order harmonic power ratio can be obtained when the phase imbalance of the 90° hybrid coupler used in the DPol-DPMZM based OSSB modulator is within ±3° and an RF modulation index is less than 0.8. The large fundamental to second order harmonic power ratio in the two new OSSB modulators leads to a high multioctave spurious free dynamic range (SFDR) performance in a long-haul fibre optic link.

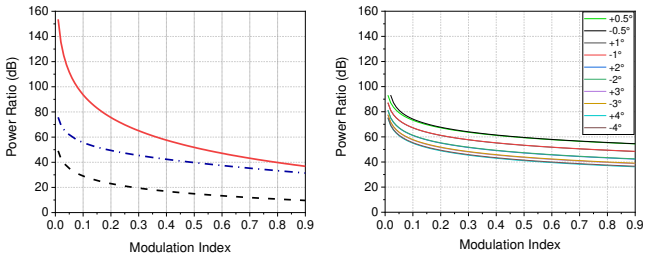

Fig. 3. (a) Simulated output RF signal to second order harmonic power ratio versus RF modulation index for the OSSB modulator based on a DP-MZM (red solid line) and the conventional OSSB modulator based on a DDMZM (black dashed line). Simulated DP-MZM based OSSB modulator output RF signal to second order harmonic power ratio versus RF modulation index for ε=30 dB and α=0.05 (blue dash-dotted line). (b) Simulated output RF signal to second order harmonic power ratio versus RF modulation index for the OSSB modulator based on a DPol-DPMZM with a 90° hybrid coupler having different phase imbalances.

	Configuration	All-optical Approach	2nd Order Sideband Suppression	3rd Order Sideband Suppression
[1]	DDMZM + 90° coupler	×	×	✓
[3]	PM with OBPF	✓	×	×
[15]	DP-MZM + 90° coupler	×	×	✓
[16]	Two cascaded PolMs + 90° coupler	×	×	×
[7]	DDMZM + 120° coupler	×	✓	×
[8]	DP-DDMZM + 90° coupler + 180° coupler	×	✓✓	✓
Current work	DP-MZM with OBPF	✓	✓✓	×
Current work	DPol-DPMZM + 90° coupler	×	✓✓	✓

Tab. 1. Configuration and the second and third order sideband suppression capability of the reported and proposed OSSB modulators. PM: phase modulator; OBPF: optical bandpass filter; PolM: polarisation modulator; DP-DDMZM: dual-parallel dual-drive Mach Zehnder modulator.

Table 1 shows the configuration and the second and third order sideband suppression capability of various OSSB modulators. The two conventional OSSB modulators, which are based on applying two 90° phase difference RF signals to a DDMZM [1] and using an OBPF to filter out either the upper or lower sidebands [3], have a simple structure. However, they are unable to suppress the second order sideband. Recent reported OSSB modulators have the function of tunable optical carrier-to-sideband ratio. Two examples of this type of OSSB modulator are shown in Tab. 1 [15], [16]. They both require electrical components and cannot suppress the second order sideband. The structures presented in [7] and [8] are the only reported experimentally verified OSSB modulators that have the ability to suppress the second order sideband. While the OSSB modulator in [7] has a simple structure, it requires a 120° hybrid coupler, which is not a standard electrical component. The OSSB modulator in [8] can suppress both the upper and lower second order sidebands as indicated by two ticks in Tab. 1. However, it needs 90° and 180° hybrid couplers. Additionally, the ratio of the RF signal power into the two DDMZMs needs to be adjusted as the RF modulation index changes to maintain second order sideband suppression. As can be seen from Tab. 1, the new DP-MZM and DPol-DPMZM based OSSB modulators do not generate both upper and lower second order sidebands. The former has a simpler structure and is free of electrical components. However, a second order harmonic component is generated after photodetection due to the presence of the third order sideband. Nevertheless, its amplitude is much smaller than that generated by the conventional DDMZM based OSSB modulator. The second order harmonic power can be further reduced by using the DPol-DPMZM based OSSB modulator as it does not generate the third order sideband under an ideal situation. This has the trade-off of more complex and expensive structure and requiring a 90° hybrid coupler with small phase imbalance.

IV. Experimental Results

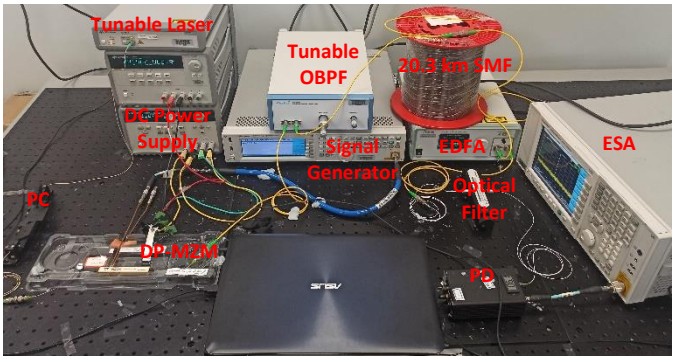

Fig. 4. Photograph of the DP-MZM based OSSB modulator experimental setup. PC: polarisation controller; OBPF: optical bandpass filter; SMF: single mode fibre; PD: photodetector; ESA: electrical signal analyser.

Experiments were conducted to verify the concept of the new OSSB modulators. The DP-MZM based OSSB modulator was set up as shown in Fig. 4 using a tunable laser (Keysight N7711A), a polarisation controller (PC) followed by a DP-MZM (Sumitomo T.SBXH1.5-20PD-ADC), a tunable OBPF (Alnair Labs BVF-300CL) and a PD (Discovery Semiconductors DSC30S). An erbium-doped fibre amplifier

This article has been accepted for publication in a future issue of this journal, but has not been fully edited. Content may change prior to final publication. Citation information: DOI 10.1109/JPHOT.2021.3123168, IEEE Photonics Journal

(EDFA) and a 0.5 nm 3-dB bandwidth optical filter were also employed to compensate for the system loss and to suppress the amplified spontaneous emission noise. Continuous wave light generated by the tunable laser source had a wavelength of 1550 nm and an optical power of 13 dBm. It was aligned to the slow axis via the PC before launching into the DP-MZM. A 13 GHz RF signal from a microwave signal generator (Keysight N5173B) was applied to the RF port of MZM_A inside the DP-MZM. Two DC power supplies were used to provide DC voltages to bias the sub and main MZMs of the DP-MZM at the desired operating points given in Section II. The optical spectrum before and after the tunable OBPF were measured on an optical spectrum analyser (OSA) (Anritsu MS9740A) with a resolution bandwidth of 0.03 nm and a span of 1 nm. Fig. 5(a) shows the measured optical spectrum at the DP-MZM output for different input RF signal powers. The corresponding modulation indexes are 0.2, 0.5 and 0.9. An optical carrier and the first and third order sidebands can be seen in the figures. The second order upper and lower sidebands were eliminated. Fig. 5(a) also shows the OBPF magnitude response has a sharp edge roll off, which largely suppresses the upper sidebands as shown in Fig. 5(b). Note that the horizontal axis on the OSA display is in wavelength. Therefore, upper sideband suppression in wavelength corresponds to lower sideband suppression in frequency. The experimental result demonstrates the realisation of OSSB modulation without the second order sidebands. The single sideband RF modulated optical signal was amplified by an EDFA. The average optical power into the PD was 8 dBm. A 26.5 GHz bandwidth electrical signal analyser (Keysight N9000A) was connected to the PD output to display the system output electrical spectrum.

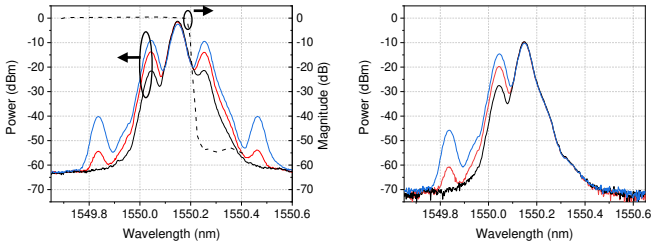

Fig. 5. Optical spectrum measured (a) before and (b) after the tunable OBPF in the DP-MZM based OSSB modulator for an RF modulation index of 0.2 (black line), 0.5 (red line) and 0.9 (blue line). The dashed line is the measured normalised tunable OBPF magnitude response.

Fig. 6(a,top) and 6(b,top) show the system output electrical spectrum at around the fundamental and second order harmonic frequency when the RF modulation index is 0.5. A high fundamental to second order harmonic power ratio of 43.5 dB can be seen from the figures. A 20.3 km long standard SMF was inserted after the tunable OBPF. The EDFA gain was adjusted so that the average optical power into the PD was around 8 dBm, which is similar to that without having a long SMF. The system output electrical spectrums at around the fundamental and second order harmonic frequency are shown in the bottom part of Fig. 6. This shows there is only little change in the output RF signal power from -14.6 dBm to -14.7 dBm after a 20.3 km SMF is inserted into the system. The same apply to the power of the second order harmonic component at 26 GHz. The experimental results demonstrate even with the inclusion of a long SMF for signal transmission, an over 40 dB fundamental to second order harmonic power ratio can still be achieved and chromatic dispersion has little effect on the DP-MZM based OSSB modulator harmonic distortion performance.

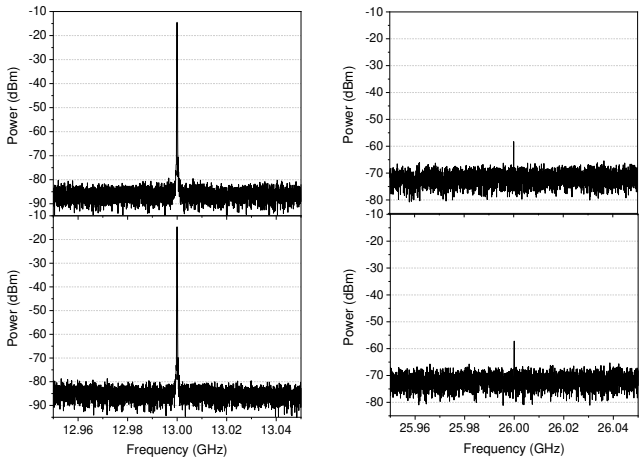

Fig. 6. Measured DP-MZM based OSSB modulator output electrical spectrum at around (a,top) the fundamental and (b,top) the second order harmonic frequency. The corresponding spectrums ((a,bottom), (b,bottom)) after a 20.3 km long standard SMF inserted into the system.

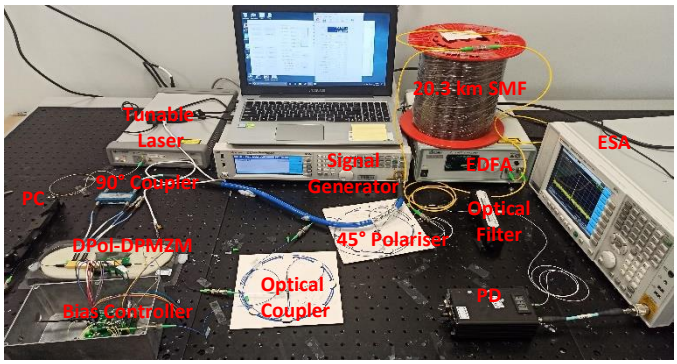

Fig. 7. Photograph of the DPol-DPMZM based OSSB modulator experimental setup. PC: polarisation controller; SMF: single mode fibre; PD: photodetector; ESA: electrical signal analyser.

Next, the DPol-DPMZM based OSSB modulator was set up as shown in Fig. 7. This was done by replacing the DP-MZM and the tunable OBPF in the DP-MZM based OSSB modulator experiment with a DPol-DPMZM (Fujitsu FTM7977HQA) and an in-line polariser with a 45° angle to the slow axis. A 2-18 GHz bandwidth 90° hybrid coupler (Krytar 1830) was used to split a 13 GHz RF signal from a microwave signal generator before applying to $DP\text{-}MZM_X$ inside the DPol-DPMZM as shown in Fig. 2(a). The two RF ports of $DP\text{-}MZM_Y$ were terminated by 50 Ω terminators. A small portion of the modulator output optical signal was fed to a modulator bias controller (PlugTech MBC-DPIQ-02) via a 5/95 coupling ratio polarisation maintaining optical coupler. The modulator bias controller provided DC bias voltages to bias the MZMs inside

This article has been accepted for publication in a future issue of this journal, but has not been fully edited. Content may change prior to final publication. Citation information: DOI 10.1109/JPHOT.2021.3123168, IEEE Photonics Journal

the DPol-DPMZM at the desired operating points. The 5/95 optical coupler was followed by the 45° in-line polariser. The average optical power into the PD was kept at around 8 dBm via adjusting the EDFA gain.

Fig. 8 shows the optical spectrum measured at the output of the 45° in-line polariser for different RF modulation indexes. This clearly shows the DPol-DPMZM based OSSB modulator output optical signal contains a carrier, the first order lower sideband and the third order upper sideband. The third order lower sideband appears for a high RF modulation index of 0.9. This is due to the 90° hybrid coupler phase imbalance as was discussed in Section II. The amplitude of the third order lower sideband is much smaller than that in the DP-MZM based OSSB modulator shown in Fig. 5(b). Note that Fig. 8 also shows a small second order upper sideband, which is due to bias errors in the DPol-DPMZM. This second order upper sideband is 38.9 dB below the first order lower sideband. The dominant unwanted sideband is the third order upper sideband, which agrees with theory. The power ratio of the fundamental to third order upper sideband is 39.8 dB and 34.7 dB for 0.5 and 0.9 RF modulation index respectively.

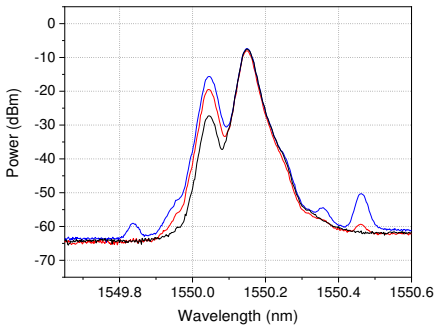

Fig. 8. Optical spectrum measured after the 45° in-line polariser in the DPol-DPMZM based OSSB modulator for an RF modulation index of 0.2 (black line), 0.5 (red line) and 0.9 (blue line).

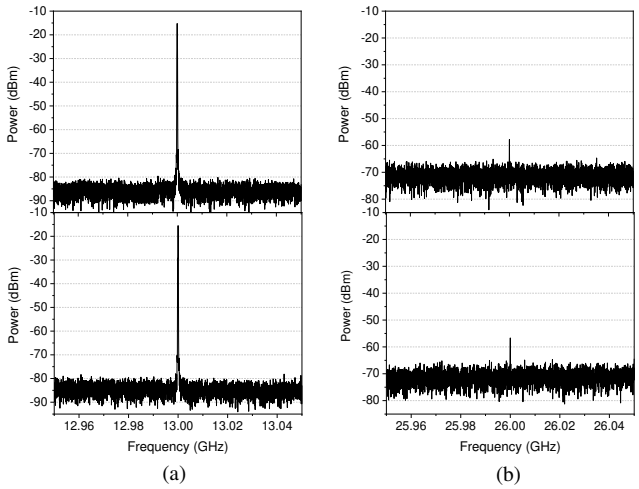

Fig. 9. Measured DPol-DPMZM based OSSB modulator output electrical spectrum at around (a,top) the fundamental and (b,top) the second order harmonic frequency. The corresponding spectrums ((a,bottom), (b,bottom)) after a 20.3 km long standard SMF inserted into the system.

The input RF signal power was adjusted to set the RF modulation index to be 0.5. Fig. 9 shows the DPol-DPMZM based OSSB modulator output electrical spectrums at around the fundamental and second order harmonic frequency without and with a 20.3 km SMF in the system. Note that the EDFA gain was adjusted so that the average optical power into the PD was 8 dBm. As shown in the figure, the output RF signal power is slightly reduced from -15.2 dBm to -15.5 dBm and the second order harmonic component power is slightly increased from -57.8 dBm to -56.7 dBm after inserting a 20.3 km SMF into the system. The power ratio of the output RF signal to the second order harmonic component is 42.6 dB and 41.2 dB without and with the 20.3 km SMF respectively. Note that the presence of the second order harmonic component is mainly due to the 90° hybrid coupler phase imbalance, which generates a small unwanted first order upper sideband that beats with the wanted first order lower sideband at the PD.

The conventional OSSB modulator based on a DDMZM was set up for comparison. This was done by replacing the DPol-DPMZM and the 45° in-line polariser with a DDMZM (Fujitsu FTM7937EZ). The DDMZM was biased at the quadrature point and was driven by two 90° phase difference RF signals from the same 90° hybrid coupler used in the DPol-DPMZM based OSSB modulator experiment. Fig. 10 shows the DDMZM based OSSB modulator output optical spectrum for different modulation indexes. This clearly shows both the second order upper and lower sidebands are present at the output of the conventional OSSB modulator. They are 29 dB, 21.8 dB, and 16.8 dB below the first order lower sideband for 0.2, 0.5 and 0.9 RF modulation index respectively.

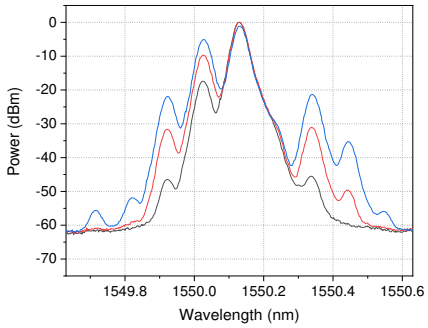

Fig. 10. Measured DDMZM based OSSB modulator output optical spectrum for an RF modulation index of 0.2 (black line), 0.5 (red line) and 0.9 (blue line).

Both the input RF signal power and the EDFA gain were adjusted so that the RF modulation index was 0.5 and the average optical power into the PD was 8 dBm. The system output electrical spectrums in Fig. 11 show 0.8 dB reduction in the output RF signal power and 23.9 dB increase in the second order harmonic power after inserting a 20.3 km SMF into the system for signal transmission. This shows using the conventional OSSB modulator in a long-haul fibre optic link has the second order harmonic distortion problem. The experimental results in Fig. 6, 9 and 11 show a large >20 dB reduction in the second order harmonic component while the

This article has been accepted for publication in a future issue of this journal, but has not been fully edited. Content may change prior to final publication. Citation information: DOI 10.1109/JPHOT.2021.3123168, IEEE Photonics Journal

output RF signal power remains almost the same in the two new OSSB modulators.

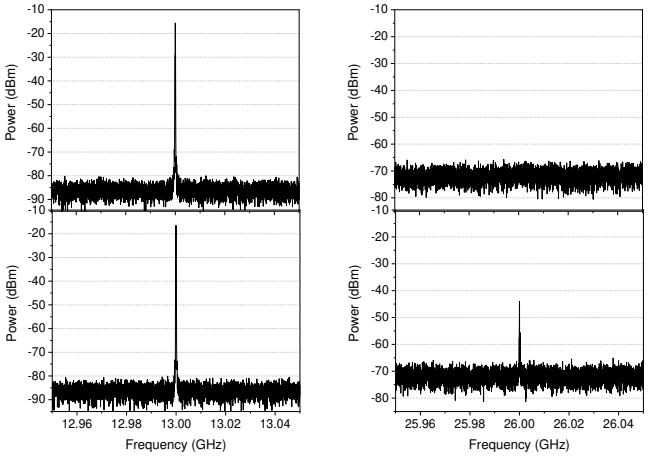

Fig. 11. Measured DDMZM based OSSB modulator output electrical spectrum at around (a,top) the fundamental and (b,top) the second order harmonic frequency. The corresponding spectrums ((a,bottom), (b,bottom)) after a 20.3 km long standard SMF inserted into the system.

The second order harmonic distortion performance of the three OSSB modulators were investigated for different input RF signal frequencies. A 20.3 km SMF was included in the system for signal transmission. The input RF signal power was adjusted so that the RF modulation index was fixed at 0.5. Fig. 12 shows the OSSB modulator based on a DP-MZM (red circle) and a DPol-DPMZM (green triangle) have more than 36 dB fundamental to second order harmonic power ratio over an input RF signal frequency range of 3 GHz to 13 GHz. The upper frequency was limited by the 26.5 GHz bandwidth electrical signal analyser used in the experiment. The reduction in the DP-MZM based OSSB modulator power ratio at 3 GHz is due to the magnitude response of the tunable OBPF used to suppress the upper sidebands has a finite edge roll off. Since the conventional DDMZM based OSSB modulator generates two second order sidebands and the phases of these two sidebands change with frequencies after a long SMF, a frequency-dependent fundamental to second order harmonic power ratio was obtained as shown by the black squares in Fig. 12. The figure also shows the simulated fundamental to second order harmonic power ratio obtained using (7) and (8). Close agreement between the measured and predicted power ratio can be seen. The experimental result reveals the second order harmonic component is 17.7 dB below the output RF signal for an input RF signal frequency of 7 GHz. The results in Fig. 12 also show, for a 7 GHz input RF signal, the DP-MZM based OSSB modulator has 22.1 dB fundamental to second order harmonic power ratio improvement compared to the conventional DDMZM based OSSB modulator. This agrees with the simulated power ratio improvement of 24.8 dB obtained from the difference between the dashed and dash-dotted lines shown in Fig. 3(a) at 0.5 modulation index.

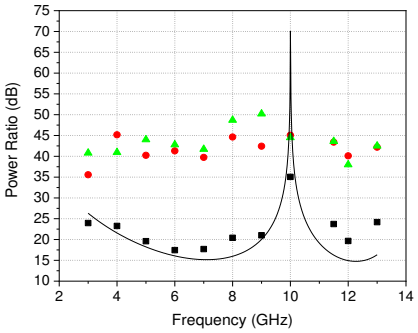

Fig. 12. Ratio of the output RF signal power to the second order harmonic power versus the input RF signal frequency for the OSSB modulator based on a DDMZM (black square), a DP-MZM (red circle) and a DPol-DPMZM (green triangle) with a 20.3 km SMF for signal transmission. Simulated output RF signal to second order harmonic power ratio of a fibre optic link formed by a DDMZM based OSSB modulator and a 20.3 km SMF (solid line).

V. Conclusion

Two OSSB modulation structures without generating the second order sidebands have been presented. They mainly comprise a laser source, an off-the-shelf optical modulator and a photodetector. They can be used to improve the multioctave SFDR performance in a long-haul fibre optic link and to reduce measurement errors in an optical vector analyser, thanks to the elimination of the second order sidebands. The two OSSB modulators are implemented by standard off-the-shelf components. The DP-MZM based OSSB modulator is free of electrical components. The DPol-DPMZM based OSSB modulator has the ability to eliminate the second order harmonic component after photodetection. The fundamental to second order harmonic power ratio for the two structures have been investigated. The two OSSB modulators were experimentally verified. The second order sidebands were eliminated in the DP-MZM based OSSB modulator. A small second order sideband with an amplitude of 38.9 dB below the first order sideband was observed at the output of the DPol-DPMZM based OSSB modulator for a high RF modulation index of 0.9. It can be suppressed by using a 90° hybrid coupler with a small phase imbalance. Both OSSB modulators have over 40 dB fundamental to second order harmonic power ratio for a 13 GHz input RF signal frequency. The power ratio remains around 40 dB for different input RF signal frequencies even with a 20.3 km SMF inserted into the system. Experimental results also show the conventional DDMZM based OSSB modulator operating under same condition as the two new OSSB modulators has small and frequency-dependent fundamental to second order harmonic power ratio.

References

[1] G. H. Smith, D. Novak, and Z. Ahmed, "Overcoming chromatic-dispersion effects in fiber-wireless systems incorporating external modulators," *IEEE Trans. Microwave Theory Tech.*, vol. 45, no. 8, pp. 1410-1415, 1997.

[2] O. Morozov, I. Nureev, A. Sakhabutdinov, A. Kuznetsov, G. Morozov, G. Il'In, S. Papazyan, A. Ivanov, and R. Ponomarev "Ultrahigh-resolution optical vector analyzers," *Photonics*, vol. 7, no. 1, 14, 2020.

[3] J. S. Fandino, M. Rius, J. Mora, P. Munoz, and J. Capmany, "Optical single sideband transmitter using phase modulation and a photonic

integrated filter," *2013 IEEE International Topical Meeting on Microwave Photonics (MWP)*, pp. 154-157, 2013.

[4] V. J. Urick, J. F. Diehl, M. N. Draa, J. D. McKinney, and K. J. Williams, "Wideband analog photonic links: some performance limits and considerations for multi-octave implementations," *Proc. SPIE*, vol. 8259, pp. 825904, 2012.

[5] Octane Wireless, "Pharad introduces 50 GHz RF photonic transmitter and receiver," 2014. [Online] Available: www.octanewireless.com/

[6] M. Xue, Y. Zhao, X. Gu, and S. Pan, "Performance analysis of optical vector analyzer based on optical single-sideband modulation," *J. Opt. Soc. Am. B,* vol. 30, no. 4, pp. 928-933, 2013.

[7] M. Xue, S. Pan, and Y. Zhao, "Optical single-sideband modulation based on a dual-drive MZM and a 120° hybrid coupler," *J. Lightwave Technol*., vol. 32, no. 19, pp. 3317–3323, 2014.

[8] E. H. W. Chan, C. Huang, and C. B. Albert, "Optical single sideband modulator without second order sidebands," *IEEE Photon. J*., vol. 10, no. 3, pp. 1-10, 2018.

[9] H. Keshavarz, S. E. Hosseini, and H. Abiri, "Low-drift AM–PM based optical single-sideband modulator without 2nd-order sideband with adjustable optical carrier-to-sideband ratio," *Optics Communications*, vol. 438, pp. 126-131, 2019.

[10] H. Keshavarz, S. E. Hosseini, H. Abiri, K. Jamshidi, and D. Plettemeier, "Bias-free silicon-based optical single-sideband modulator without 2nd-order sideband," *IEEE Photon. J*., vol. 12, no. 4, pp. 1-16, 2020.

[11] M. Milosavljevic, M. P. Thakur, P. Kourtessis, J. E. Mitchell, and J. M. Senior, "Demonstration of wireless backhauling over long-reach PONs," *J. Lightwave Technol*., vol. 30, no. 5, pp. 811-817, 2012.

[12] A. Wootten and A. R. Thompson, "The Atacama large millimeter/submillimeter array," *Proceedings of the IEEE*, vol. 97, no. 8, pp. 1463-1471, 2009.

[13] S. Shimotsu, S. Oikawa, T. Saitou, N. Mitsugi, K. Kubodera, T. Kawanishi, and M. Izutsu, "Single side-band modulation performance of a $LiNbO_3$ integrated modulator consisting of four-phase modulator waveguides," *IEEE Photon. Tech. Lett*., vol. 13, no. 4, pp. 364-366, 2001.

[14] T. Kawanishi, "Precise optical modulation and its application to optoelectronic device measurement," *Photonics*, vol. 8, no. 5, 160, 2021.

[15] B. Hraimel, X. Zhang, Y. Pei, K. Wu, T. Liu, T. Xu, and Q. Nie, "Optical single-sideband modulation with tunable optical carrier to sideband ratio in radio over fiber systems," *J. Lightwave Technol*., vol. 29, no. 5, pp. 775–781, 2011.

[16] Y. Zhang, F. Zhang, and S. Pan, "Optical single sideband modulation with tunable optical carrier-to-sideband ratio," *IEEE Photon. Tech. Lett*., vol. 26, no. 7, pp. 653-655, 2014.